Journal of Alloys and Compounds 509 (2011) 7931–7936

Contents lists available at ScienceDirect

Journal of Alloys and Compounds

journal homepage: www.elsevier.com/locate/jallcom

Synthesis, structural and magnetic characterization of nanocrystalline nickel ferrite—$NiFe_2O_4$ obtained by reactive milling

T.F. Marinca[a,b], I. Chicinaş[a,*], O. Isnard[b], V. Pop[c], F. Popa[a]

[a] Materials Sciences and Technology Department, Technical University of Cluj-Napoca, 103-105 Muncii Avenue, 400641 Cluj-Napoca, Romania
[b] Institut Néel, CNRS, Université Joseph Fourier, 25 rue des Martyrs, 38042 Grenoble, France
[c] Faculty of Physics, Babes-Bolyai University, 1 M. Kogalniceanu St., 400084 Cluj-Napoca, Romania

ARTICLE INFO

Article history:
Received 7 April 2011
Received in revised form 9 May 2011
Accepted 11 May 2011
Available online 19 May 2011

Keywords:
Nanocrystalline materials
Magnetization
Reactive milling
Nickel ferrite

ABSTRACT

Nanocrystalline nickel ferrite ($NiFe_2O_4$) has been synthesized from a stoichiometric mixture of oxides NiO and α-Fe_2O_3 in a high energy planetary mill. An annealing at 350 °C, after milling, was used to improve the solid state reaction. The obtained powders were investigated by X-ray diffraction, magnetic measurements, scanning electron microscopy, X-ray microanalysis and differential scanning calorimetry. The particles size distribution was analyzed using a laser particle size analyser. The nickel ferrite begins to form after 4 h of milling and continuously form up to 16 h of milling. The obtained nickel ferrite has many inhomogeneities and a distorted spinel structure. The mean crystallites size at the final time of milling is 9 ± 2 nm and the lattice parameter increases with increase the milling time. DSC measurements revealed a large exothermic peak associated with cations reordering in the crystalline structure. The magnetization of the obtained powder depends on the milling time and annealing. After the complete reaction between the starting oxides the milling reduces the magnetization of the samples. The magnetization increases after annealing, due to the reorganization of the cations into the spinel structure.

1. Introduction

Generally, all the soft magnetic ferrites are very important materials due to their magnetic and electric properties. The spinel ferrite suitable for many applications, such as: high frequency magnetic materials, recording media, ferrofluid technology, sensor technology, and microwave applications [1–5]. The soft magnetic ferrites are materials which crystallize in cubic spinel structure, spatial group *Fd*3*m*. The chemical formula of the spinel ferrite can be written as $MeFe_2O_4$, where Me is a metal or a group of metallic elements with 2 total valence. The Me^{2+} and Fe^{3+} cations can be distributed into two crystal sites of spinel structure: tetrahedral sites and octahedral sites. Typically two extreme type of spinel structure can be found: normal spinel and inverse spinel, but in practise mixed spinel structure are also observed. In normal spinel structure the tetrahedral sites are occupied by the Me^{2+} and the octahedral sites are filled by the Fe^{3+} cations. In inverse spinel structure the Fe^{3+} cations are distributed between the tetrahedral and octahedral sites and the Me^{2+} cations are found in octahedral sites. The mixed spinel structure has the cations distributed in a combined mode between the normal and inverse structure. The magnetic and electric properties of the soft ferrite are closely related to their intra-crystalline ordering of the cations [6,7].

Nickel ferrite ($NiFe_2O_4$), like all soft magnetic ferrites, is the subject of intense researches in recent years. Nickel ferrite obtained by equilibrium methods has an inverse spinel structure with the Fe^{3+} cations equally distributed between the two kinds of sites, Ni^{2+} cations being located in octahedral sites and the magnetic ordering in the spinel structure of $NiFe_2O_4$ is ferrimagnetic. The iron cations from tetrahedral sites have the magnetic moments coupled antiparallel with the magnetic moments of nickel and iron from octahedral sites [6]. It was highlighted that in the nanocrystalline/nanostructured state nickel ferrite has magnetic properties which differ from the polycrystalline state [8–10]. In order to produce nickel ferrite in nanocrystalline/nanostructured state several methods such as sol–gel [11,12], solvothermal [13], co-precipitation [14], bottom up [15], microemulsion [16] or hydrothermal [17] are used. Beside those methods the mechano-chemical synthesis route is a useful method for producing the nickel ferrite in nanocrystalline state. For producing the nanocrystalline nickel ferrite by mechano-chemical synthesis two ways are used: (i) in the first one, the ferrite is formed in the nanocrystalline state by solid state reaction between precursors during milling [9,18–20]; (ii) in the second one, the polycrystalline nickel ferrite obtained by other methods is milled in order to reduce the grain size and to refine the structure [10,21,22]. Several studies where reported regarding the producing of nanocrystalline nickel

* Corresponding author. Tel.: +40 264 401705; fax: +40 264 415054.
E-mail address: Ionel.Chicinas@stm.utcluj.ro (I. Chicinaş).

0925-8388/$ – see front matter © 2011 Elsevier B.V. All rights reserved.
doi:10.1016/j.jallcom.2011.05.040

ferrite by mechano-chemical route, but the results are very different depending on the experimental conditions. For example, the nickel ferrite phase was obtained after 8 h [20] or else after 35 h of milling [21]. For the sample milled 8 h a heat treatment was applied in order to increase the formation of nanoferrite [20]. Another study reported the obtaining of nickel ferrite in the nanocrystalline state by mechanical milling (with a crystallite size of 9 nm) from a mixture of oxides [2]. In the same article, it was observed that the magnetization is reduced by milling. A non-equilibrium distribution of cations and a spin canted effect have been reported by the same authors [2]. The cations inversion between the tetrahedral and octahedral sites into the spinel structure alongside of the spin canted effect and superparamagnetic behaviour was also reported by other authors [23]. The magnetization of nickel ferrite obtained in nanocrystalline state by mechanical milling is lower than the magnetization of nickel ferrite obtained by ceramic method [23]. Finally, it is worth to note that mechanical/reactive milling can be used to obtained nanostructures that have a non-equilibrium distribution of cations within the crystal structure.

The present paper presents the results regarding the synthesis of nanocrystalline nickel ferrite by reactive milling starting from an equimolar mixture of commercial oxides and the characterization of some structural and magnetic properties.

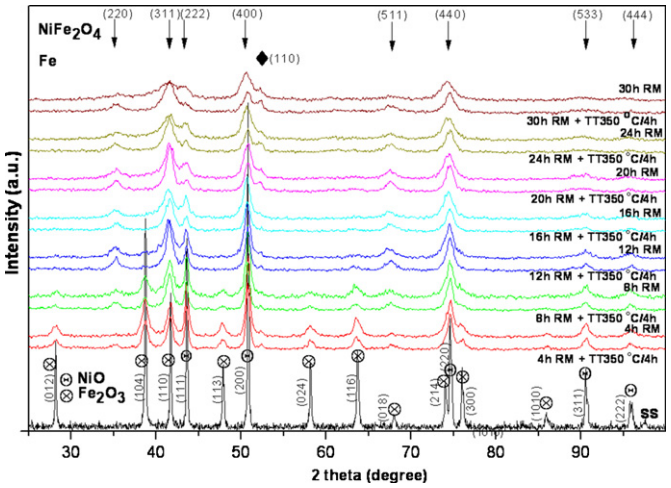

Fig. 1. X-ray diffraction patterns of the starting sample (ss), as-milled samples (4, 8, 12, 16, 20, 24 and 30 h of milling) and for the milled and subsequently annealed at 350 °C for 4 h samples. The position of the diffraction peak for each phase is indicated in the figure. For clarity, the diffraction patterns where vertically shifted.

2. Experimental

A mixture of high purity commercial oxides powders (Alpha Aesar), nickel oxide (NiO—bunsenite) and iron oxide (α-Fe_2O_3—hematite) in molar ratio of 1:1 was used as starting sample. Stainless steel vials and balls were used for the milling process in high energy planetary mill Pulverisette 4 (Fritsch). The ball to powder mass ratio was 15:1. The vial rotational speed (ω) and the disc rotational speed (Ω) were established at 800 rpm, respectively at −400 rpm. After milling, the samples were annealed in vacuum at a temperature of 350 °C for 4 h in order to remove the internal stresses induced by milling and to improve the solid state reaction.

The formation of nickel ferrite by milling was investigated by X-ray diffraction (XRD) in the angular range $2\theta = 25–100°$ using a Siemens D5000 diffractometer which operates in reflection with CoK_α radiation ($\lambda = 1.7903$ Å). The mean crystallite size was calculated using Scherrer's formula from full-width-at-half maximum (FWHM) of the diffraction peaks for the milled and annealed samples [24]. The lattice parameter was determined using Celref 3 program [25].

The morphology and chemical homogeneity of the particles were studied by scanning electron microscopy (SEM) using a JEOL—JSM 5600-LV microscope, equipped with energy dispersive spectrometer (Oxford Instruments, INCA 200 software). The particle size distribution has been determined using a Laser Particle Size Analyzer (Fritsch Analysette 22–Nanotec) with an analysis field of 10 nm to 2000 μm.

Differential scanning calorimetry (DSC) investigations were performed using an alumina reference sample in NETZSCH–DSC 404S apparatus. The temperature range was between 25 and 1000 °C and a heating/cooling speed of 10 °C/min was used. The measurements were performed in Ar atmosphere in order to avoid the supplementary air oxygen.

The magnetization curves, $M(H)$, were recorded at room temperature using the extraction sample method in a continuous magnetic field of up to 8 T [26]. The spontaneous magnetizations values have been derived from an extrapolation to zero field of the magnetization obtained in the magnetic field higher than 5.5 T.

3. Results and discussion

The X-ray diffraction patterns of the as-milled samples and those milled and subsequently annealed are shown in Fig. 1 (RM – as-milled samples and RM + TT 350 °C/4 h – milled and subsequently annealed samples). For comparison, in the same figure is also shown the diffraction pattern for the starting mixture (SS). The Bragg reflections corresponding to the nickel ferrite ($NiFe_2O_4$) are noticed in the diffraction pattern after 4 h of milling, the $NiFe_2O_4$ (2 2 0) and (5 1 1) peaks are clearly visible in the diffraction patterns at this time of milling. Those peaks are not the most intense peaks corresponding to the spinel nickel ferrite, the most intense peaks ((3 1 1) and (4 4 0)) are overlapped with the nickel oxides diffraction peaks. A broadening of the diffraction peaks of the precursors oxides, due to the decreasing of the crystallites sizes and to the second-order internal stresses induced by milling can be observed. A significant quantity of nickel ferrite was formed after 4 h of milling. By increasing milling time, the diffraction peaks of the nickel ferrite are more clearly visible and those of the precursor oxides decrease.

The most intense diffraction peak of the hematite phase (2 0 0) peak, is almost invisible after 12 h of milling. By increasing the milling time at 16 h, the diffraction peaks corresponding to the nickel and iron oxides are no more present in the diffraction patterns; this indicates that the reaction between the precursors nickel and iron oxides is completed. The diffraction peaks intensity of the nickel ferrite phase does not follow the expectations reference JCPDS file (10-0325). This highlights that nickel ferrite formed by milling has many inhomogeneities and is very disordered comparison to the ordered reference. The nickel ferrite structure is far from equilibrium (inverse spinel structure), the spinel is rather a mixed one instead of a complete inverse. These results are in good agreement with earlier reported results [9]. By increasing the milling time, the system is getting far from equilibrium conditions and the nickel ferrite mixed spinel structure evolves continuously up to 30 h of milling.

After only 4 h of milling the (1 1 0) iron peak can be observed in the diffraction patterns. The iron peak intensity increases by increasing the milling time. This is a consequence of the powder contamination during milling with iron from the milling vial and balls [27]. After annealing, the diffraction peaks definition is better, the nickel ferrite peaks intensity are closer to the reference JCPDS file and the intensity of the peaks corresponding to the precursors oxides are reduced. This is due to the fact that the annealing removes the internal stresses induced by milling and increase the crystalline state of the synthesized $NiFe_2O_4$ powder. For the milling time up to 12 h, where the $NiFe_2O_4$ is not completely formed, the annealing improves also the reaction between the milled and unreacted precursor oxides [28]. In Fig. 2 is presented the fit and deconvolution of the XRD patterns for hematite (1 0 4) peak and nickel ferrite (2 2 0) peak for the 8 h milled sample, before and after annealing. The nickel ferrite (2 2 0) peak is much better defined after annealing in comparison with the peak before annealing. Also, the ratio between the integral intensities of the hematite (1 0 4) maximum and nickel ferrite (2 2 0) maximum is decreasing from 2.33 before annealing at 1.02 after annealing. So, the amount of nickel ferrite formed after annealing is significant.

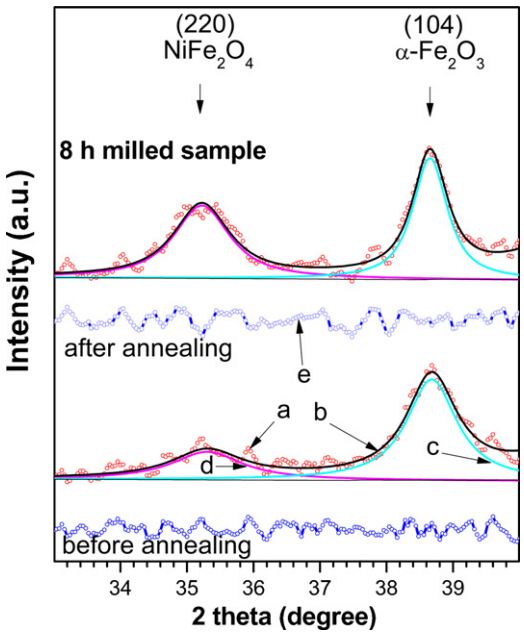

Fig. 2. The fit and deconvolution of XRD patterns for the hematite (1 0 4) maximum and nickel ferrite (2 2 0) maximum, for the 8 h milled sample, before and after annealing. (a) Experimental XRD points; (b) the best fit curve of the XRD experimental points; (c) hematite (1 0 4) maximum obtained by deconvolution; (d) nickel ferrite (2 2 0) maximum obtained by deconvolution; (e) difference between the experimental points and the corresponding fit.

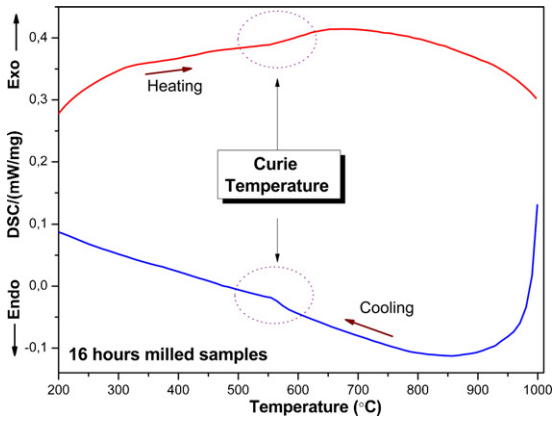

Fig. 4. DSC heating and cooling curves for the sample milled 16 h. The peaks corresponding to the magnetic transition of the $NiFe_2O_4$ on the heating and cooling curves are marked.

The evolution of the mean crystallite size and of the lattice parameter for the as-milled samples and respectively for milled and annealed samples versus milling time are shown in Fig. 3. The crystallite size is typically in nanometer range: 39 ± 2 nm for 12 h of milling and decreases rapidly by increasing the milling time, up to 9 ± 2 nm after 30 h of milling. The lattice parameters for the as-milled and for the milled and subsequently annealed samples increase by the increasing of the milling time. The lattice parameter of the as-milled samples is larger than for the milled and annealed samples, due to the internal stresses induced by milling and a non-equilibrium cations distribution in spinel structure. After annealing, the internal stresses are removed, a lattice relaxation occurs and it is possible to have a partial re-ordering of the metallic ions between tetrahedral and octahedral sites [29]. Whatever the milling time, the internal stresses and the ionic disorder lead to a larger lattice parameter of the milled ferrites than that of the nickel ferrite obtained by the ceramic method ($a = 8.339$ Å, JCPDS 10-0325 file). Another cause of the increased lattice parameter could be the higher iron content in the ferrite due to the iron contamination during milling. Indeed iron atoms could be incorporated into the nickel ferrite spinel structure. So, it is possible to have a nickel ferrite with more iron cations. Further investigations in order to clarify this aspect are in progress.

DSC curves recorded both on heating and cooling for the sample milled for 16 h is shown in Fig. 4. On the heating curve is remarked a large exothermic peak between 200 and 1000 °C. Released heat is associated with the lattice relaxation and with the cations reordering between tetrahedral and octahedral sites. Beside the large exothermic peak, on the heating curve an endothermic peak can be also remarked. This endothermic peak is associated with the Curie

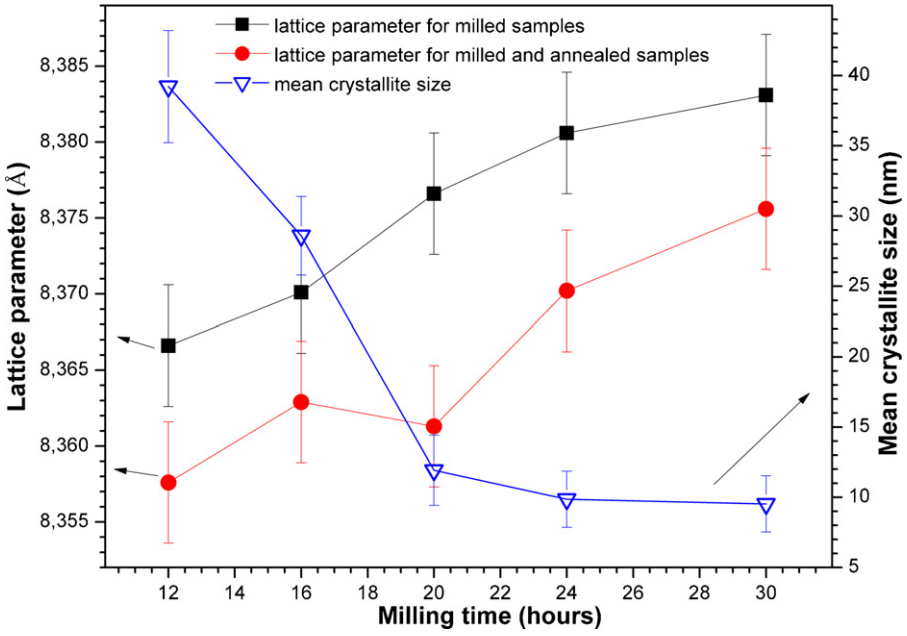

Fig. 3. Evolution of the mean crystallite size and of the lattice parameter of the $NiFe_2O_4$ for as-milled samples and respectively for milled and annealed samples versus milling time.

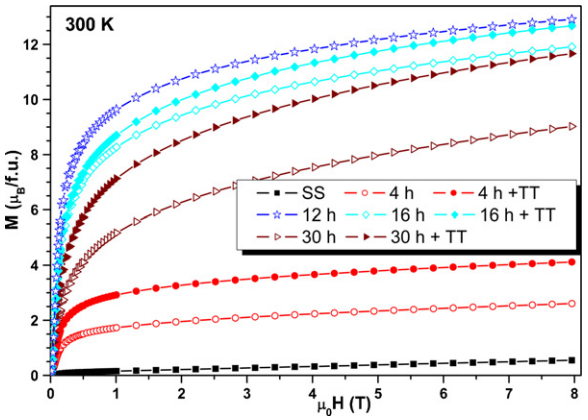

Fig. 5. Room temperature magnetization curves of the starting sample, 4, 12, 16 and 30 h milled samples and milled and subsequently annealed (350 °C/4 h) samples.

temperature of the nickel ferrite. The certainty that this peak is corresponding to the magnetic transition of nickel ferrite is given by the appearance of an exothermic peak at the same value (560 °C) on the cooling curve. The peak corresponding to the magnetic transition on the heating curve is larger, due to the distorted structure of the ferrite. Also the value of the magnetic transition temperature is lower compared with the values determined for the nickel ferrite synthesized by classical ceramic route (585 °C) [6]. The structure of the obtained spinel ferrite and probably the impurities leads to a lower magnetic transition temperature.

The magnetization measurements also indicate a change in the structure of the processed particles during the milling. The magnetization curves $M(H)$ for the starting mixture, as-milled samples and milled and annealed samples are shown in Fig. 4. The $M(H)$ curves recorded for the milled sample are characteristic for a ferro- and ferrimagnetic order. Typically the magnetic ordering in spinel nickel ferrite is ferrimagnetic [8]. The magnetic moments of the cations from tetrahedral sites are coupled antiparallel with the moments of the cations from octahedral sites. The magnetization is influenced by the disordered spinel structure produced by milling [9]. It may be noted that even for a magnetic field of 8 T the magnetization is not completely saturated (Fig. 5). This behaviour could be attributed to the following phenomena: (i) the spin canted effect on the surface of the particles; (ii) a superparamagnetic behaviour due to very fine particles of ferrite obtained by milling and (iii) a combination of the two previously [8–10]. The $M(H)$ curves of the milled samples are not saturated even after the annealing. Probably the spin canted effect is very strong and it is not removed completely by the annealing and/or the un-saturated magnetization is caused in major part by the superparamagnetismn of the very fine particles.

The evolution of the spontaneous magnetization calculated for the starting sample (SS), as-milled samples and for the milled and annealed samples versus milling time is given in Fig. 6. The formation of an important quantity of nickel ferrite after 4 h of milling is confirmed by the magnetic analysis; the spontaneous magnetization is 1.95 μ_B/f.u. at this time of milling. For samples milled up to 12 h, the spontaneous magnetization increases continuously by increasing milling time and it is reaching 10.84 μ_B/f.u., as a consequence of the increased amount of ferrite phase in the material. After 16 h of milling, when very probable the reaction between the precursor oxides is finished, the spontaneous magnetization decreases by increasing milling time. The spontaneous magnetization reaches 6.22 μ_B/f.u. at the end of the milling process, after 30 h. The magnetization values are lower in comparison with the value obtained for the nickel ferrite synthesized by ceramic route and in comparison with the calculated one [6,9]. These lower values could be attributed to the non-equilibrium distribution of the cations in spinel structure, structural disorder and spin canted/superparamagnetism effect [2,8–10].

After annealing, the spontaneous magnetization increases in comparison with the magnetization of the as-milled samples. For the milling times where the $NiFe_2O_4$ is not completely formed the magnetization increases due the increasing of the amount of spinel phase in material. For example, the spontaneous magnetization for the 4 h milled sample increases at 3.42 μ_B/f.u. after annealing. All the factors favouring the reduction of the magnetization (non-equilibrium cations distribution, structural defects) for the samples

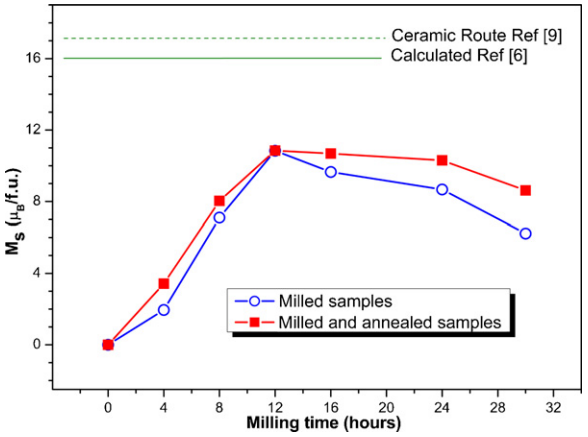

Fig. 6. Spontaneous magnetization of the starting sample, 4, 8, 12, 16, 20, 24 and 30 h milled samples and of the milled and subsequently annealed (350 °C/4 h) samples. For comparison some values from the literature are given.

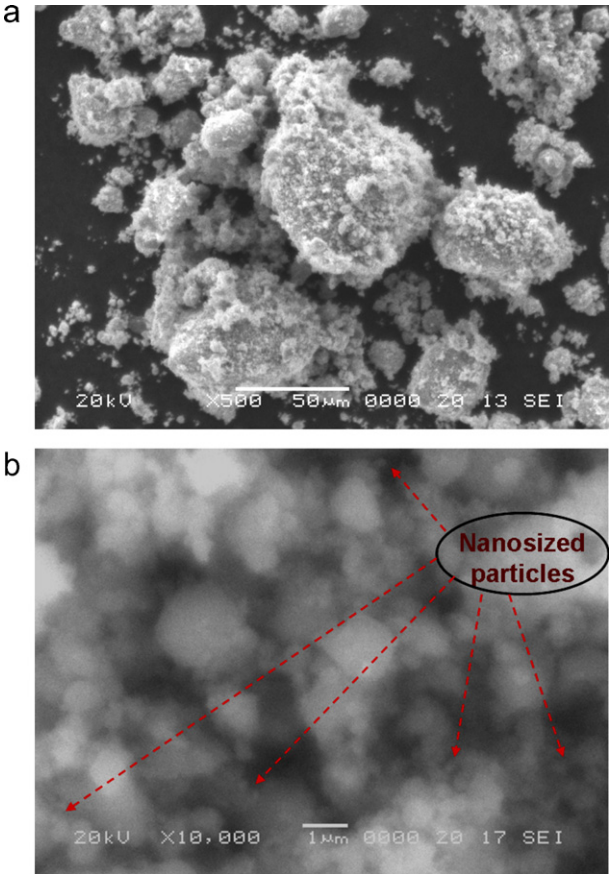

Fig. 7. SEM images of nickel ferrite powders obtained for the 16 h milled sample: (a) 500× and (b) 10,000×. The powder is formed by agglomeration of nanometric particles alongside by micrometric size particles.

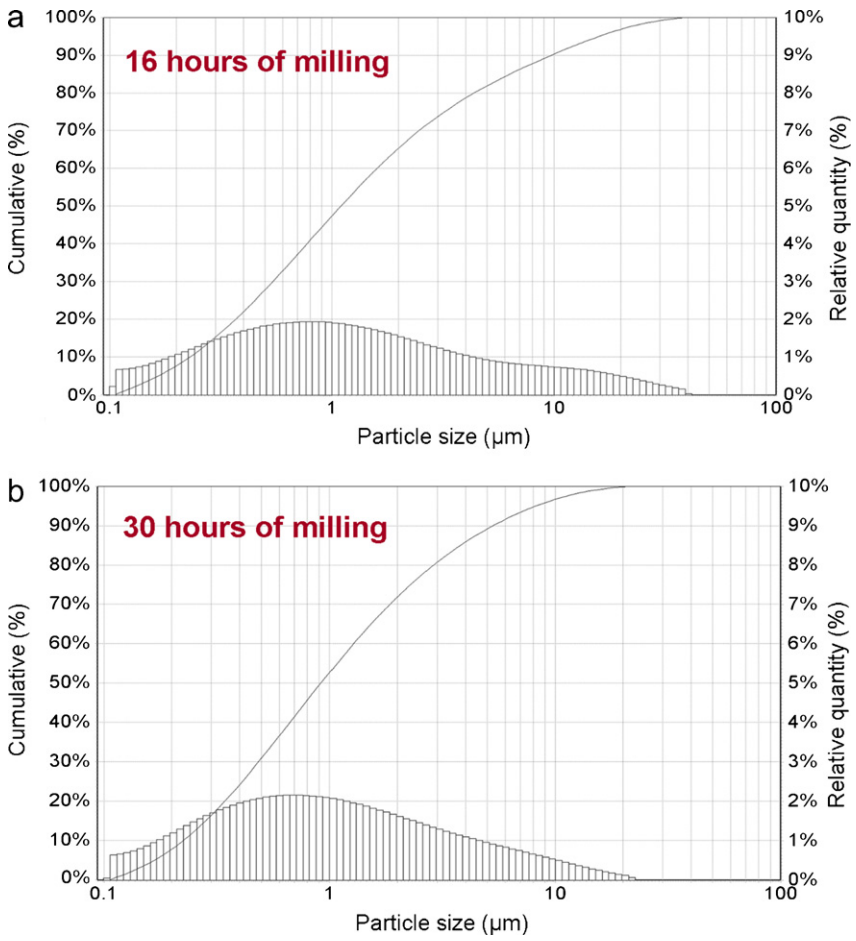

Fig. 8. Particles size distribution of $NiFe_2O_4$ powder obtained after 16 h of milling (a) and respectively, 30 h of milling (b).

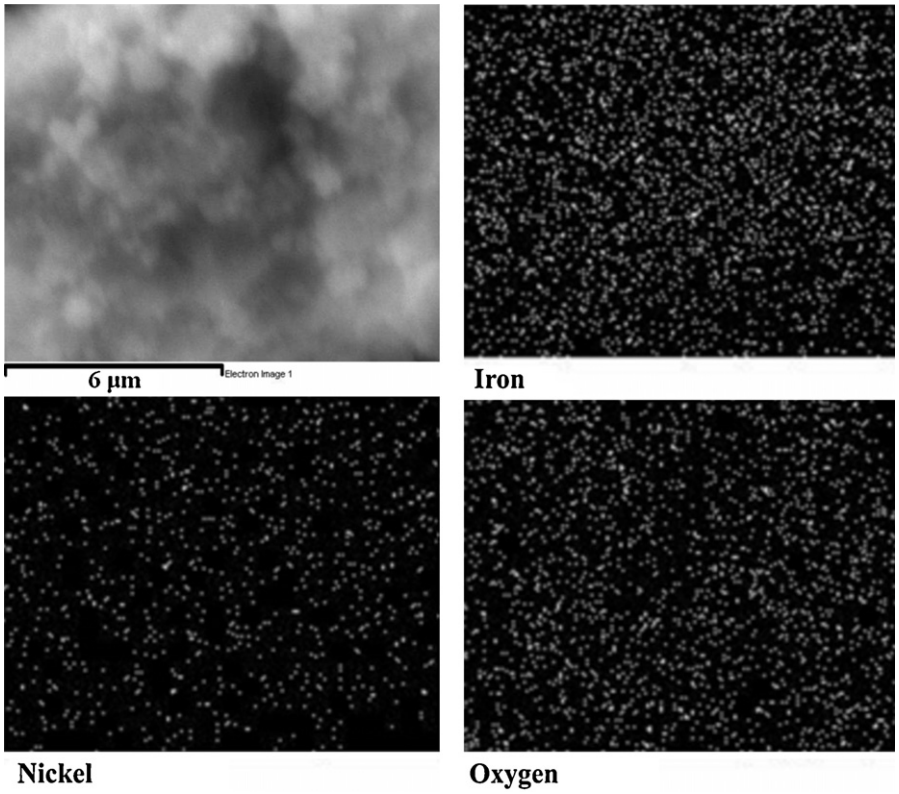

Fig. 9. Distribution maps for Ni, Fe and O chemical elements obtained for the 16 h milled sample. The X-ray microanalysis was performed on the SEM image presented in the upper left side (10,000×).

where the $NiFe_2O_4$ was completely formed are removed or reduced by annealing, so the nickel ferrite is little closer to equilibrium and the crystallinity is increased [30]. The spontaneous magnetization is increasing after annealing with about 11%, from 9.65 μ_B/f.u. to 10.68 μ_B/f.u. for the 16 h milled sample.

The SEM studies show that the particles have a polyhedral shape; the powder is formed by agglomeration of nanometric particles alongside by micrometric size particles. In Fig. 7 is presented a SEM images obtained for the 16 h milled sample at a magnification of 500× and 10,000×. Very fine particles can be the single-domain particles with higher magnetization [6]. The particle size distribution analyses confirmed the details obtained by SEM. There are particles of a few micrometers and particles whose size is in nanometric range. The median particle size D_{50} determined for the 16 h milled sample is 1.1 μm and decreases by increasing the milling time up to 0.92 μm after 30 h of milling. In Fig. 8a and b is presented the particles size distributions for the 16 h milled sample and 30 h milled sample, respectively.

The EDX microanalyses confirmed the results obtained by XRD, which indicate a contamination of the samples with elemental iron. Whereas the starting sample EDX analysis indicated an iron/nickel ratio of 2:1, this ratio increases upon increasing the milling time. The amount of iron impurities is increasing upon increasing the milling time. For the 8 h milled sample the Fe:Ni atomic ratio is increasing at 2.2–2.3:1 and after 16 h of milling the atomic ratio of 2.45–2.6:1 is reached. This ratio becomes 2.6–2.8:1 for the sample milled for 30 h. These ratios correspond to a powder contamination with iron between 3 and 10%. Small amount of elemental chromium was also detected by X-ray microanalyses. The chromium impurities are provided by the vial material which is consisting of stainless steel with 20% of chromium. The contamination with chromium varying with the analyzed micro-areas and increases by increasing the milling time. The amount of chromium detect in the sample is about 0.3–0.4% at for the sample milled 8 h and reaches at 1% for the 30 h milled samples.

The samples are chemically homogeneous and iron is uniformly distributed in the milled powder. In Fig. 9 is presented the EDX micro-analyses obtained for a micro-area from 16 h milled sample. The chemical homogeneity is maintained upon increasing the milling time.

4. Conclusions

The nanocrystalline nickel ferrite was successfully obtained by reactive milling from a stoichiometric mixture of commercial nickel and iron oxides. After 16 h of milling the reaction between precursor oxides is finished. The nickel ferrite is formed and supports structural changes continuously up to 30 h of milling. A very disordered nickel ferrite, with many defects was obtained by milling. The annealing improves the solid state reaction of the nickel ferrite formation, removes the internal stresses and reduces the structural defects. The mean crystallite size decreases with increasing milling time, up to 9 ± 2 nm after 30 h of milling. The lattice parameter decreases after annealing due to the spinel structure relaxation. DSC measurements revealed a large exothermic process associated with cations reordering in the crystalline structure. The magnetization is influenced by the disordered ferrite structure and by the internal stresses induced during milling. The formation of the spinel ferrite increases the magnetization, after the complete formation the magnetization decreases. The spontaneous magnetization increases after annealing for all the milling time, due to the reorganization of the cations into the spinel structure. A possible superparamagnetic component can be induced in the magnetization by very fine powder particles. The SEM images and particles size analysis confirmed the existence of very fine nickel ferrite particles. The processed powder was contaminated with iron and chromium from the vials and balls.

The reactive milling and subsequently annealing is an efficient route to synthesize nanocrystalline nickel ferrite powder. Further experiments in order to increase the magnetization, without losing the nanocrystalline state are in progress.

Acknowledgment

This work was supported by CNCSIS – UEFISCSU, project number PNII – IDEI code 1519/2008.

References

[1] R.C. Kambale, P.A. Shaikh, S.S. Kamble, Y.D. Koleka, J. Alloys Compd. 478 (2009) 599–603.
[2] V. Šepelák, I. Bergmann, A. Feldhoff, P. Heitjans, F. Krumeich, D. Menzel, F.J. Litterst, S.J. Campbell, K.D. Becker, J. Phys. Chem. C 111 (2007) 5026–5033.
[3] S.M. Patange, S.E. Shirsath, B.G. Toksha, S.S. Jadhav, K.M. Jadhav, J. Appl. Phys. 106 (2009) 023914.
[4] J. Ding, X.Y. Liu, J. Wang, Y. Shi, Mater. Lett. 44 (2000) 19–22.
[5] N. Ponpandian, P. Balaya, A. Narayanasamy, J. Phys.: Condens. Matter 14 (2002) 3221–3237.
[6] B.D. Cullity, C.D. Graham, Introduction to Magnetic Materials, 2nd ed., IEEE Press & Wiley, New Jersey, 2009.
[7] A. Goldman, Modern Ferrite Technology, 2nd ed., Springer, Pittsburgh, 2006.
[8] R.H. Kodama, A.E. Berkowitz, E.J. McNiff Jr., S. Foner, Phys. Rev. Lett. 77 (2) (1996) 394–397.
[9] V. Šepelák, S. Indris, P. Heitjans, K.D. Becker, J. Alloys Compd. 434–435 (2007) 776–778.
[10] C.N. Chinnasamy, A. Narayanasamy, N. Ponpandian, K. Chattopadhyay, K. Shinoda, B. Jeyadevan, K. Tohji, K. Nakatsuka, T. Furubayashi, I. Nakatani, Phys. Rev. B 63 (2007) 184108.
[11] D. Carta, M.F. Casula, A. Falqui, D. Loche, G. Mountjoy, C. Sangregorio, A. Corrias, J. Phys. Chem. C 113 (2009) 8606–8615.
[12] A.T. Raghavender, K. Zadro, D. Pajic, Z. Skoko, N. Biliškov, Mater. Lett. 64 (2010) 1144–1146.
[13] B. Baruwati, S.V. Manorama, Mater. Chem. Phys. 112 (2008) 631–636.
[14] J. Jacob, M.A. Khadar, J. Appl. Phys. 107 (2010) 114310.
[15] B. Baruwati, K.M. Reddy, S.V. Manorama, R.K. Singh, O. Parkash, Appl. Phys. Lett. 85 (4) (2004) 2833–2835.
[16] R.D.K. Misra, A. Kale, B.J. Kooi, J.T.M. De Hosson, Mater. Sci. Technol. 19 (2003) 1617–1621.
[17] H. Kavas, A. Baykal, M.S. Toprak, Y. Köseoğlu, M. Sertkol, B. Aktaş, J. Alloys Compd. 479 (2009) 49–55.
[18] M. Jalaly, M.H. Enayati, P. Kameli, F. Karimzadeh, Physica B 405 (2010) 507–512.
[19] Č. Jovalekić, M. Zdujić, A. Radaković, M. Mitrić, Mater. Lett. 24 (1995) 365–368.
[20] H. Yang, X. Zhang, W. Ao, G. Qiu, Mater. Res. Bull. 39 (2004) 833–837.
[21] M.E. Arani, M.J.N. Isfahani, M.A. Kashi, J. Magn. Magn. Mater. 322 (2010) 2944–2947.
[22] V. Šepelák, D. Baabe, K.D. Becker, J. Mater. Synth. Process. 8 (5/6) (2000) 333–337.
[23] V. Šepelák, M. Menzel, I. Bergmann, M. Wiebcke, F. Krumeich, K.D. Becker, J. Magn. Magn. Mater. 272–276 (2004) 1616–1618.
[24] P. Scherrer, Nachr Gött Matematisch Phys Klasse I (1918) 98–100.
[25] J. Laugier, B. Bochu, CELREF V3. Developed at the Laboratoire des Matériaux et du Génie Physique, Ecole Nationale Supérieure de Physique de Grenoble (INPG), 2003, http://www.inpg.fr/LMGP.
[26] A. Barlet, J.C. Genna, P. Lethuillier, Cryogenics 31 (1991) 801–805.
[27] T.F. Marinca, I. Chicinaş, C.V. Pricǎ, F. Popa, Mater. Sci. Forum 672 (2011) 145–148.
[28] V. Pop, O. Isnard, I. Chicinaş, J. Alloys Compd. 361 (2003) 144–152.
[29] S. Bid, S.K. Pradhan, Mater. Chem. Phys. 84 (2004) 291–301.
[30] V. Šepelák, D. Baabe, D. Mienert, D. Schultze, F. Krumeich, F.J. Litterst, K.D. Becker, Magn. Magn. Mater. 257 (2003) 377–386.